Journal of the Serbian Chemical Society
JSCS-info@shd.org.rs • www.shd.org.rs/JSCS
J. Serb. Chem. Soc. *90* (3) 351–367 (2025)
JSCS–5392
Original scientific paper
Published 24 March, 2025

Corrosion studies, parameter effects, and surface morphology of AA5052-AA6101T6 friction stir welded joints

SATHISH RENGARAJAN[1], G. KASIRAJAN[2]* and R. ASHOK KUMAR[3]

[1]Department of Mechanical Engineering, St. Joseph's College of Engineering, Semmancheri, Chennai, Tamil Nadu-600119, India, [2]Research Scholar, Department of Mechanical Engineering, St. Joseph's College of Engineering, Semmancheri, Chennai, Tamil Nadu--600119, India and [3]Department of Mechanical Engineering, SRM Madurai College for Engineering and Technology, Nedungulam Main Rd, Pottapalayam, Tamil Nadu-630611, India

(Received 17 April, revised 19 May, accepted 24 August 2024)

Abstract: Traditional fusion welding is unsuitable for welding aluminum alloys because secondary brittle phases, porosity, and cracks are likely to form as the alloy solidifies. Friction stir welding (FRSTW), a new solid-state welding method, can join similar or dissimilar aluminium (ALU) alloys. In this study friction stir welded AA5052-AA6101T6 alloy samples were tested for corrosion characteristics. The microstructure and mechanical behavior of FRSW--welded AA5052-AA6101T6 ALU alloy joints were examined relative to input parameters. Microstructure reveals that welding speed and rotation-speed affect the weld microstructure analyzed sample welded areas. Twenty-nine samples were corrosion tested in 3.5 % NaCl, household water (880 ppm – SPM), 1 M H_2SO_4, 1 M NaOH and natural seawater for 72 h. Domestic salt water and acid medium showed better resistance to corrosion than alkaline and salt media. Impedance studies demonstrated slight anodic and cathodic potential changes after friction stir welding.

Keywords: microstructure; aluminum alloys; impedance study; weight loss method.

INTRODUCTION

Aluminum (ALU) alloys are more thermally stable than steel and can withstand temperatures between 480–660 °C before melting. Aluminum has corrosion resistance properties high strength-to-weight ratios, and excellent thermal and electric conductivity in maritime conditions. Also, it provides good characteristics such as lightweight, machinability, non-magnetic, formability and ductility are some of the qualities of this material.[1] Fabrication of weldments can be done by using either pressure or non-pressure welding techniques, depending on the

* Corresponding author. E-mail: gurukasirajan@gmail.com
https://doi.org/10.2298/JSC240417078R

technology employed. Generally, ALU alloys provide a protective oxide layer during the joining process due to this protection these alloys were used in several applications like vehicles, marine applications and overhead transmission lines.[2] One of the solid-state joining processes called friction stir welding (FRSTW) was developed quite a while ago. Subsequently, it has been demonstrated as a successful technique for joining chemically dissimilar aluminum alloys compositional compatibility is not an issue, unlike in fusion welding and any aluminum alloy can be welded.[3–7] At low energy, FRSTW exhibited numerous mechanical benefits, including superior dimensional stability, repeatability, absence of alloying loss and fine microstructure at the joints.[8] Dynamic recrystallization produces a fine grain structure in the weld region's center, which affects the joint strength. Corrosion resistance is an inherent property of aluminum; nevertheless, the thickness can vary due to internal and external factors. When compared to the various metal welding techniques, aluminum welding is used to make a longer design because aluminum is more resistant to corrosion than steel. The breakdown of materials, most often metals, caused by chemical reactions with the environment, leading to a component’s functional failure, is known as corrosion. Environmental concentration, stress, erosion and temperature are the four variables that determine corrosion, a form of reverse extractive metallurgy. Huge yearly economic losses from 1 to 5 % of GNP are caused by it for all nations. Hence, the materials and their corrosion behaviour in different atmospheres are receiving research interest.[38] Also, the corrosion studies on FRSTW aluminium samples have stated the importance of corrosion studies on the welded samples for mechanical applications.[9–13] The reported work stated that the polarization resistance and potential voltage were both low when the CR of the base material welded zones of the metals such as AA5083 and AA7023 were immersed in an artificial NaCl solution. The disparity in volta potential readings led to a higher current density in the AA7023 base material and a strongly attacked border between the two materials.[14] Most of the researchers have reported the FRSTW parameters and the procedures of five, six and seven series of ALU alloys with its characterization.[39] In addition to the weight reductions already mentioned, the corrosion resistances offered by the passive aluminum oxide layer are still another major perk of switching from steel to aluminum components. This research identified the research gap of the distinct alloys such as AA5052 and AA6101-T6 stir welded joints tensile strength and corrosion behavior in a different corrosive medium such as acid, alkali, 1 M salt solution, domestic water, and natural seawater to know the mechanical suitability. Present work also investigated the parameters effect of FRST welded test samples between AA5052 and AA6101-T6 using microstructure analysis. Followed by the sample’s tensile strength, corrosion resistivity in different environments is analyzed for the mechanical applications purpose.

EXPERIMENTAL

Materials and methods

The samples AA5052 and AA6101-T6, which were friction stir welded, were made according to the methods described in earlier research.[15] Friction stir butt welding was performed on AA5052 and AA6101-T6, 6 mm thick using an FRSTW machine depicted in Fig. 1a–c. The shoulder pin length is 5.7 mm with a hexagonal shape of 2.5 mm on 6 six sides the geometrical dimension and welded samples are shown in Fig. 1d and e. Twenty-nine experiments were carried out based on Four process parameters with three levels using response surface methodology.

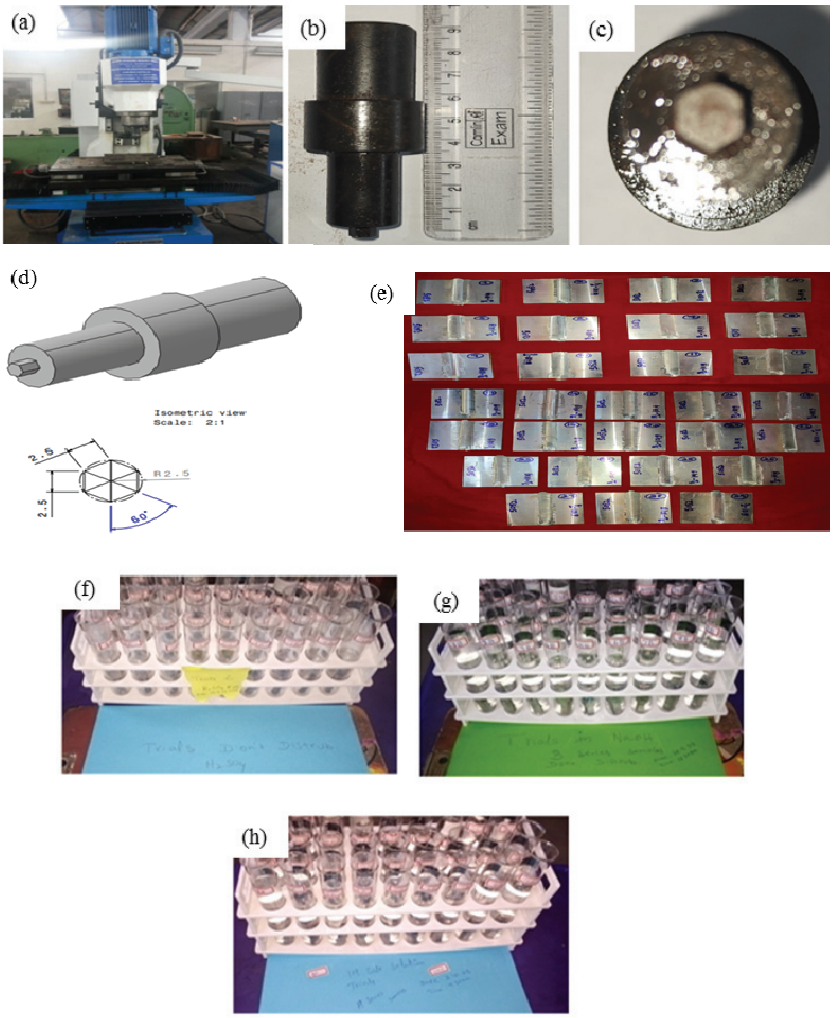

Fig. 1. a) Welding machine, b) spindle tool dimension, c) ALU spinner of FRSTW process, d) pin profile dimension, e) welded samples prepared FRSTW test samples in: f) 1 M H_2SO_4, g) 1M NaOH and h) 1 M salt solution for weight loss investigation.

The dissimilar plates are clamped on two sides, the rotating tool is made to contact till its shoulder, now the tool traverse takes place the materials reach its localized heating, a plastic deformation takes place at the interface of the material, and mechanical pressure is applied to make the weld joint. The tensile test was taken in UTM with 5-ton capacity with Fuel Instruments and engineers with a digital encoder. For microstructural studies metallurgical microscope is an inverted trinocular metallurgical microscope with 50–80× magnification, with paired eye pieces which have 12 V with a polarizer prism. The microscope is attached to a 5 MP camera. The selected test samples welded joints nature is investigated by XRD technique.[16,17] XRD patterns between 2θ 10–80.48 were recorded under continuous scan mode in Bruker-binary V4 (RAW) model at 25 °C with Cu as anode material and the fixed generator settings of 30 mA, 40 kV, respectively. X-Ray diffraction (XRD) test was conducted at 3 kW power with a focus size of 0.4 mm×12 mm Cu anode; the system should also be able to work with other X-ray sources like Mo, Co, Fe or Cr.

The natural salt corrosive medium seawater was collected near the Chennai port, Tamil Nadu, India, and used as such for the corrosion studies. Similarly, domestic fresh water collected from Karasangal, Kancheepuram District, Chennai, Tamil Nadu, India. Both natural mediums were used for the corrosion test in boiling tube.

The welding plate samples were degreased in acetone before being alkaline imprinted in 7.5 wt. % NaOH at 55–60 °C for 5 min. Following this, they were rinsed with distilled water in preparation for corrosion testing. The samples were then subjected to acidification in different prepared corrosion solutions such as 1 M of sodium hydroxide solution (40 g in 1000 mL of distilled water), 1 M H_2SO_4 (28 mL of 37.5 % in 1 L), 1 M commercial sodium chloride crystals solution, domestic hard water (*SPM* = 880 ppm) and marine water.[18,19] The cleaned test specimens were immersed in prepared and collected corrosive medium for 72 h (3 days). After that the welded samples were dried in sunlight and hot air drier for 5 min. Then, the samples were weighed in digital weighing balance. The trials conducted in various corrosive medium are presented in Fig. 1f. From the weight loss data**,** average weight loss was calculated and used for the corrosion rate measurement.

The observed weight losses were recorded and the average weight loss in each corrosive medium was calculated. Using average weight loss corrosion rate was calculated using the following formula (1):

$$R = \frac{534 \times WL}{\rho A t} \tag{1}$$

where R is corrosion rate in mpy, WL is weight loss in g, ρ is density of the metal, g/cm^3, A is surface area in in^2, and t is time in h.

The design surface area is calculated using the formula 2*lb*:

$$\text{Total surface area} = 2(1\times3 + 1.5\times0.5) + 0.5\times3 = 2(3+0.75) + 1.5 = 9 \text{ cm}^2 \tag{2}$$

Potentiometric study

FRSTW test samples were evaluated using a conventional calomel electrode to detect anodic behavior and its impact. This study also tested a galvanic cell with the same calomel electrode in a corrosive artificial 3.5 % salt solution and found higher weight loss. The EIS describes electrolyte resistance, adsorption, diffusion, charge transfer resistance, double-layer capacitance and unique phase processes and features. After surface improvement with emery papers, the trial samples' corrosion behavior was examined using the well-known EIS method. A working electrode (WE) was submerged in a corrosive salt medium after washing the sur-

face in a polar solvent mixture of water and acetone. A saturated calomel electrode (SCE) recorded anodic and corrosion behavior. The corrosion rate was tested in hydrochloric acid. After setting the surface area to 1 cm^2, density to 2.71 g/cm^3, open circuit potential to –0.72839 V, and reference potential to 0.241 V at 25 °C, potentiodynamic data were recorded. The Tafel plot was plotted and the corrosion rate was calculated using the I_{corr} value.

RESULTS AND DISCUSSION

Tensile test

The welded samples were polished well and designed for tensile tests like the dog bone model based on ASTM standards. The specimen (Fig. 2a and b) was tested using forces up to the model breakage. The outcomes of the test samples revealed low to higher tensile strength values. Out of 29 samples, sample 13 showed lower tensile strength of 92 MPa. Likely, sample 26 exposed higher tensile strength (137 MPa). From Table I, a moderate value of 112 MPa was observed for sample 4. The tensile strength results were analyzed along with welded parameters. The selected specimen number 9 (1200 rpm and 7 kN) exposed somehow better strength for a single pass. At the same time, the tensile strength increased with increasing traverse speed and axial load which exhibited the tensile strength of 94 MPa. The applied parameters and their outcomes are presented in Table I. Sample 13 exposed low tensile strength due to higher rpm with a single pass. The results showed that the number of passes affect the material mechanical property which includes tensile strength but the remaining parameters must be optimized for the future design. Next, this work analyzed the rpm with tensile strength. A higher rpm of 1400 with the axial load 7 kN exhibited a tensile strength of 124 MPa. When compared with the 8 kN double pass sample, the triple pass showed good tensile strength. The tensile strength of the sample's rpm has followed the increasing order as follows: sample 7 (80, 7, 1400, 3, 124) > sample 8 (80, 7, 1000, 3, 130) > sample 26 (80, 6, 1200, 3, 137). From the results, this work observed that the optimized rpm is 1200, force, 6–7 kN,

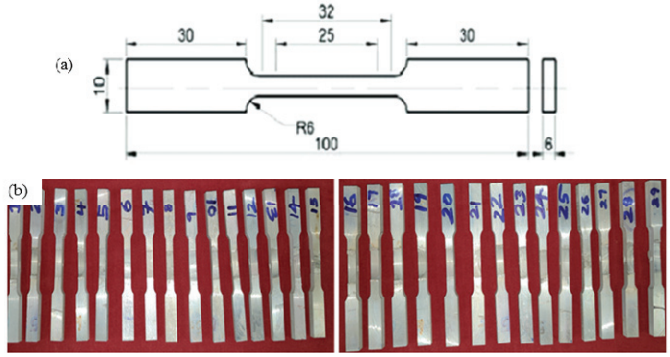

Fig. 2. Tensile strength; a) test specimen dimension; b) dog bone test specimens.

traverse speed = 80 mm/min with triple pass. The modification without changing the rpm showed good improvement in tensile strength which coincides.[20] After the tensile strength test, similar dimensions of welded zones are carried out for the corrosion test by weight loss method.

TABLE I. Tensile strength results of the prepared FRSTW test specimens

SampleNo.	Tensile stress MPa	Sample No.	Tensile stress MPa	Sample No.	Tensile stress MPa
1	114	11	97	21	94
2	109	12	115	22	108
3	104	13	92	23	105
4	112	14	117	24	93
5	126	15	107	25	115
6	123	16	118	26	137
7	124	17	121	27	116
8	130	18	113	28	110
9	99	19	106	29	129
10	111	20	103		

Characterization

The butt weld of the aluminum alloy (AA5052 and AA6101-T6) joint's surface grains nature was analyzed by morphological method. To measure the welded joints nature, this work selected sample numbers such as 1, 4, 8, 9, 13 and 26 for microstructure analysis. Fig. 3 exposed surface morphology of the selected samples such as 90 mm/min, 8 kN×1200 rpm×2 pass, 80 mm/min×7 kN×1200 rpm×2 pass, 80 mm/min×7 kN×1000 rpm×3 pass, 90 mm/min×7 kN×1200 rpm×1 pass, 80 mm/min×7 kN×1400 rpm×1 pass, and 80 mm/min×6kN×1200 rpm×3 pass specimens surface grain nature.

Fig. 3a revealed the pancakes like grains due to higher speed and force. This image revealed that the higher load and processing heat energy may be the reason for these slight cracks. The grains are of almost uniform size which may cause good durability at high temperatures. Similar size hair cracks are found in sample number 8 and 9 (Fig. 3c and d). Fig. 4f shows the lower grain size and micro-level hair cracks. Triple passes at lower RPM and lower passes with higher RPM cause uneven pancakes or hair cracks. The parameters such as higher strain, heat, and exciting strains cause distinct microstructures in FRSTW aluminum alloys. Tool-induced plastic deformation and frictional heat between plates extend grain structure before welding refines it at the junction. Due to material interaction with the shoulder, tool pin, and process factors, the "nugget", was formed on the surface. The welded zones have shown pricklier stretched microstructure in which the grains are oriented alongside the progressing direction (Fig. 3e). The microstructure has etched pits and grains slightly smaller than AA6101 aluminum alloy. Gwyddion processed image is shown in Fig. 3g.

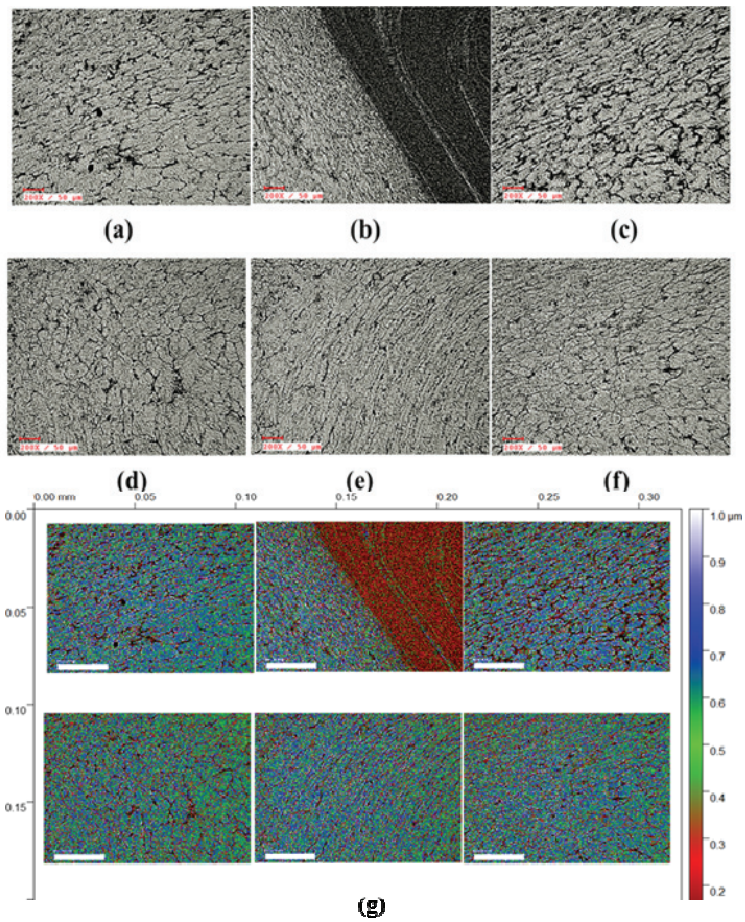

Fig. 3. Microstructure images of FRST welded test samples: a) 1, b) 4, c) 8, d) 9, e) 13, f) 26 and g) 5 Gwyddion processed microstructure images of FRST welded test samples.

Welded samples 4, 13 and 16 were XRD analyzed after microstructure characterization. The identification of alloy combinations was done using the 2θ *versus* intensity relationship. The XRD patterns of trials 4, 13 and 26 showed the composition of metals and aluminum in combination, accordingly. The XRD patterns show up at 2θ 38.66, 44.89, 65.21 and 78.33 in Fig. 4. These 2θ values validate the Al_3M molecular formula of the remaining metal elements. They verified that the welded zones of corrosion-resistant aluminum alloys were tightly bound. The results showed that the welding was stable. α-Al metallic solution phases, $MgZn_2$ and $CuAl_2$ intermetallic compounds (*hkl*) values were observed in all processed XRD patterns. The observed values from Match-3 software are presented in Table II. The values are almost coincidental with the aluminum alloys welded zone reports as shown.[21–26]

TABLE II. XRD analysis outcomes of FRSTW welded samples

Sample No.	*hkl*	2θ / °	*D* / nm
4	111	38.66	2.33
	200	44.89	2.02
	202	65.21	1.43
13	111	38.66	2.33
	200	44.89	2.02
	202	65.21	1.43
	311	78.33	1.22
26	111	38.66	2.33
	200	44.89	1.99
	202	65.21	1.41
	311	78.33	1.20

Samples were carried out for the energy dispersive analysis to identify the alloy metals present in the anodic and cathodic metals of FRSTW specimens. The energy values are compared with MA table element energy. All welded specimens have shown similar energy level peaks. The boundary region EDAX exposed the peaks at 0.02–0.073(noise), 0.64–0.73 (O K), 1.23–1.25 (Mg K), 1.46–1.51 (Al K), 1.82–1.85 (Si K), 4.9–4.99 (V or Cr), 6.31–6.4 (Fe/Mn K) and 7.1–7.2 (Fe Kβ1) keV. The obtained values are coincidental with the reported data and confirm the elements of the selected base metals compositions.[27–30] The intermetallic region exposed the Al_3Mg_2 and metal oxides of higher-composition metals. These results revealed and supported the butt-welded zone deformation with grains structure. Also, results revealed the similarities in welded zones. In addition, α-Al (FeMn) Si may be the reason for the different coarse sizes observed in the microstructure of FRSTW specimens. The deformed boundary was observed from the microstructure and confirmed by EDAX shown in Fig. 4.

Corrosion studies

The selected sample's surface area was measured and carried for the weight loss investigations by immersion technique.[40] Different corrosive mediums were selected as per the experimental discussion and the weight loss for all the samples individually. Weight loss was studied in various corrosive media. Base metals AA5052 and AA6101-T6 with other corrosion-tested aluminum welded joints after 72 h. As the sample dries, a black corrosion film covers the whole surface, and white, shiny products are created, indicating that the parent metal has low corrosion resistance. There is a great deal of variance, however, in the corrosion regions of the welding joints when subjected to various process settings. The recorded outcomes are presented in Tables III and IV. Sample 1 showed the lowest weight loss in the acid medium and sample 15 exposed higher loss in the same medium. From the observed weight loss of the 29 samples, this work calculated the average weight loss of 215 mg. Likely, this work observed the

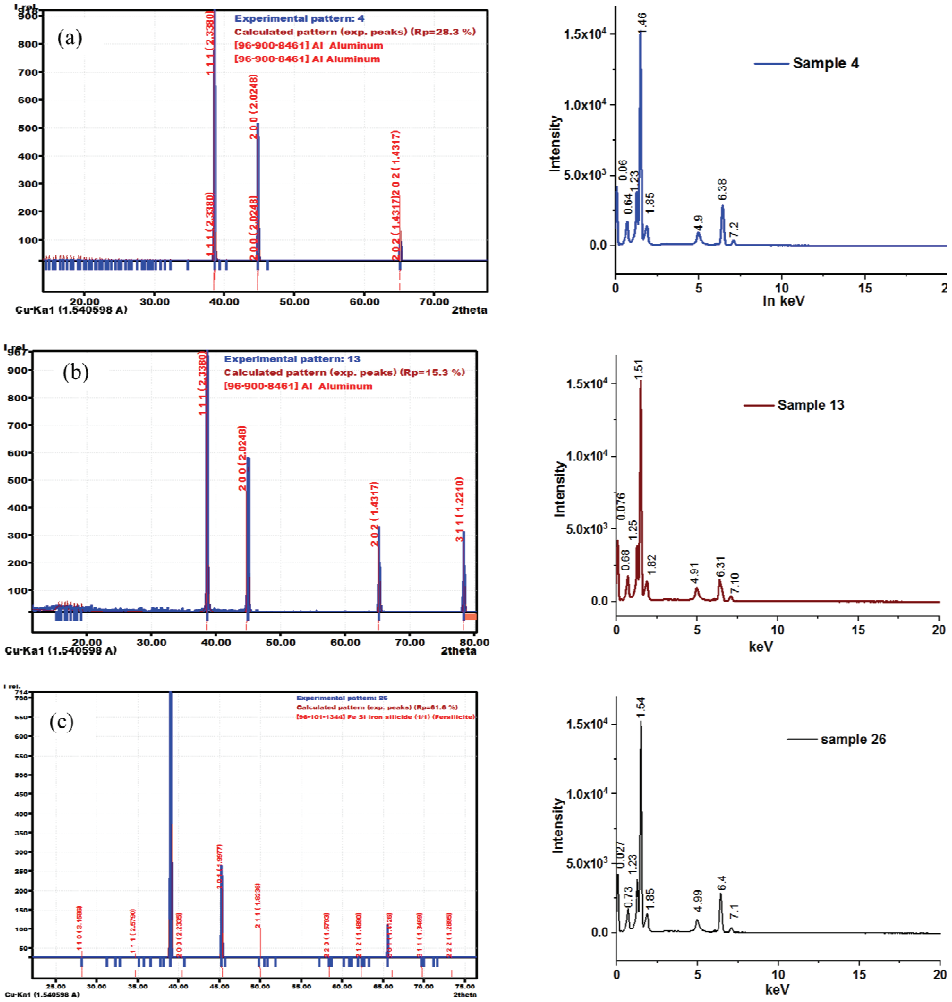

Fig. 4. XRD and EDAX images for samples: a) 4, b) 13 and c) 26.

average weight losses of the samples in the order of basic medium (S.N-27 = 397 mg; low, S.N-15 = 787 mg; high), domestic water (S.N-1 = 40 mg; low, S.N-19 = = 51 mg; high), 3.5% salt solution (S.N-27 = 597 mg; low, S.N-25 = 986 mg; high) and seawater (S.N-4 = 596 mg; low, S.N-20 = 959 mg; high). The welded joints' corrosion resistance outshines that of the underlying metal, it follows. More dislocation flaws occur during rolling because the base metal's grain size is not uniform. In contrast, the dynamic recrystallization of grain size is made possible by the strong mechanical and thermal impacts of stirring processing, which results in uniformly sized grains that are reconciled in the welding joints and, as a result, fewer defects. The corrosion resistance of the welding joints is greatly

TABLE III. Initial mass, thickness and mass loss (g) in different corrosion medium

Sample No.	Mass loss in 0.1 M acid			Mass loss in 0.1 M base			Mass loss in domestic water (SPM = 880 ppm)		
	Initial mass	Final mass	Mass loss	Initial mass	Final mass	Mass loss	Initial mass	Final mass	Mass loss
AA5052	6.213	5.987	0.226	5.231	4.479	0.752	5.890	5.677	0.213
AA6101-T6	5.468	5.186	0.282	6.475	5.648	0.827	4.996	4.878	0.118
1	6.620	6.518	0.102	6.885	6.129	0.756	6.675	6.635	0.040
2	6.680	6.499	0.181	6.910	6.194	0.716	6.700	6.686	0.014
3	6.640	6.422	0.218	6.669	6.196	0.473	6.459	6.441	0.018
4	7.060	6.865	0.195	7.057	6.483	0.574	6.847	6.824	0.023
5	6.750	6.566	0.184	6.702	6.113	0.589	6.492	6.470	0.022
6	6.690	6.496	0.194	6.857	6.071	0.786	6.647	6.632	0.015
7	5.750	5.596	0.154	6.804	6.162	0.642	6.348	6.320	0.028
8	6.600	6.323	0.277	6.949	6.263	0.686	6.493	6.463	0.030
9	6.520	6.322	0.198	6.631	5.933	0.698	6.175	6.159	0.016
10	5.800	5.593	0.207	6.951	6.164	0.787	6.495	6.465	0.030
11	6.670	6.420	0.250	5.808	5.198	0.610	5.352	5.316	0.036
12	6.690	6.392	0.298	6.531	5.989	0.542	5.212	5.186	0.026
13	6.560	6.299	0.261	6.933	6.453	0.480	6.477	6.446	0.031
14	6.820	6.621	0.199	6.534	6.017	0.517	6.078	6.045	0.033
15	6.810	6.493	0.317	5.623	5.129	0.494	5.401	5.367	0.034
16	6.720	6.439	0.281	6.733	6.245	0.488	6.511	6.473	0.038
17	6.670	6.449	0.221	6.836	6.212	0.624	6.614	6.572	0.042
18	6.550	6.365	0.185	5.980	5.485	0.495	5.674	5.628	0.046
19	6.900	6.628	0.272	6.588	5.942	0.646	6.366	6.320	0.046
20	6.870	6.736	0.134	6.721	6.240	0.481	6.499	6.449	0.050
21	6.900	6.711	0.189	6.746	5.999	0.747	6.524	6.485	0.039
22	6.430	6.180	0.250	6.851	6.224	0.627	6.173	6.129	0.044
23	6.990	6.728	0.262	6.450	6.003	0.447	6.233	6.184	0.049
24	6.590	6.466	0.124	6.086	5.669	0.417	5.869	5.819	0.050
25	6.610	6.322	0.288	5.995	5.598	0.397	5.778	5.739	0.039
26	6.330	6.120	0.210	5.993	5.446	0.547	5.899	5.858	0.041
27	5.950	5.705	0.245	7.325	6.588	0.737	7.437	7.386	0.051
28	6.550	6.392	0.158	6.918	6.148	0.770	7.030	6.985	0.045
29	6.860	6.672	0.188	6.692	6.015	0.677	6.804	6.757	0.047
Average loss	0.215			0.602					0.035

enhanced as a result of this. This work observed the average weight loss of all 29 samples such as 0.602 g (basic medium), 0.035 g (domestic water), 0.766 g (3.5% salt solution) and 0.727 g (sea water). The average weight loss of the specimens in selected corrosive mediums was lowered when compared with the source metal weight loss. Also, both salt atmospheres are showing almost similar weight loss. Corrosion of metal may and will occur in saltwater. Aluminum boats still have their uses on land, but they will require some extra care when out on

the water. Galvanic corrosion is the mechanism by which salt corrodes aluminum. When compared with the reported results, three times of weight loss was observed in salt water. Also, the difference in weight loss revealed the effect of welding parameters on surface degradation. RPM and many passes in friction stir welding are the major effects on corrosion resistivity. When comparing the mediums, the order of surface deterioration exists as follows salty domestic water < acid < alkali < sea water < artificial salt water.

TABLE IV. Initial mass, thickness and mass loss in different corrosion medium

Sample No.	Weight loss in 3.5 % salt solution			Weight loss in marine water		
	Initial mass	Final mass	Mass loss	Initial mass	Final mass	Mass loss
AA5052	4.984	4.038	0.946	6.235	5.324	0.911
AA6101-T6	6.214	5.229	0.985	6.184	5.312	0.872
1	6.745	5.919	0.826	6.241	5.468	0.773
2	7.087	6.298	0.789	6.621	5.872	0.749
3	6.760	6.087	0.673	6.323	5.673	0.650
4	6.712	5.938	0.774	6.925	6.314	0.611
5	6.820	5.961	0.859	6.585	5.769	0.816
6	6.911	6.025	0.886	6.877	6.189	0.688
7	6.762	5.920	0.842	5.853	5.257	0.596
8	6.668	5.682	0.986	6.195	5.396	0.799
9	6.964	6.126	0.838	5.868	5.055	0.813
10	7.106	6.409	0.697	5.82	5.045	0.775
11	6.275	5.414	0.861	5.928	4.969	0.959
12	6.649	5.907	0.742	6.019	5.253	0.766
13	6.715	5.767	0.948	6.471	5.629	0.842
14	6.636	5.819	0.817	6.377	5.681	0.696
15	6.532	5.738	0.794	6.673	5.935	0.738
16	6.668	5.860	0.808	6.815	6.198	0.617
17	6.456	5.747	0.709	5.984	5.273	0.711
18	6.869	6.176	0.693	6.358	5.557	0.801
19	6.156	5.310	0.846	6.401	5.659	0.742
20	6.782	6.001	0.781	6.322	5.675	0.647
21	6.281	5.556	0.725	6.218	5.594	0.624
22	6.372	5.785	0.587	6.354	5.716	0.638
23	6.667	6.050	0.617	6.142	5.423	0.719
24	6.592	5.875	0.717	6.555	5.832	0.723
25	6.559	6.022	0.537	5.931	5.25	0.681
26	6.817	6.134	0.683	6.557	5.83	0.727
27	6.459	5.834	0.625	6.056	5.3	0.756
28	6.423	5.676	0.747	6.147	5.32	0.827
29	6.959	6.157	0.802	6.442	5.839	0.603
Average loss		0.766			0.727	

Using the weight loss data, this work calculated corrosion rate in terms of miles per year (Tables V) using the above-mentioned formula (1). Observation shows the same order of the specimen's corrosion rate in selected corrosive mediums.

TABLE V. Corrosion rate of FRSTW samples from weight loss

Average mass loss, g	Medium	*M* Surface area×Eq.wt×Total h	*CR* in mpy 534×mass loss/*M*
0.215	0.1 M acid	9×2.7×72	0.066
0.602	0.1 M alkali	9×2.7×72	0.184
0.035	Domestic water	9×2.7×72	0.011
0.766	3.5 % NaCl	9×2.7×72	0.234
0.727	Sea water	9×2.7×72	0.222

From the reports, this work observed that the welded materials corrosion rates are decreased in respective medium. This work observed the similar observations when compared with base metals. This research selected the magnesium and chromium containing aluminum alloys for this novel study. When compared with the reported results for the other Al alloys, our welded samples exposed good result.

A higher corrosion rate of 0.234 miles per year was shown by the artificial salt medium when compared to the other corrosive mediums. Therefore, this study expanded to include a potentiodynamic analysis of 4, 13 and 26 specimens chosen based on their tensile strength. The potentiodynamic output data opened through corrosion view software and Tafel plots are plotted (Fig. 5). The graphical outcomes are presented in Table VI. From the table, sample 13 showed higher corrosion rate when compared with other selected samples. Even sample 4 showed lower tensile strength, it showed the corrosion rate of 3.156 mpy. This is due to the deformed welded joint of FRSTW sample. The Tafel outcome data also revealed the almost equal corrosion potential from –0.87 to –0.91 V. But, the corrosion current differed in the order of sample 26 < sample 4 < sample 13. Our sample showed 0.15 V difference with FRSTW AA6082.[31] When compared with the reported potential of aluminum (Al/Al^{3+}, –1.70 V), welded samples exposed the lowered potential.[32] The movement to more positive values indicates that the corrosion resistance of the friction stir-welded samples was improved. The lowest corrosion current density, which means the highest corrosion resistance, was observed on selected specimens. I_{corr} values exist between 781.78 and 0.52 μA. The lowest value of sample 26 showed the improvement of the corrosion resistance due to the FRSTW process as per reported values.[33] When compared with the reported results, our samples have shown slightly higher corrosion potential.[34–37] Sample 26 exhibited a lower rate due to the grain nature and cathodisation with the remaining base metal compositions. This work observed the corros-

ion resistivity in the order of sample 13 > sample 4 > sample 26. When compared the other reported corrosion researches, Table VII, this work selected AA5052 and AA6101-T6 aluminium alloys joints for future submarine-based construction and water-based designs.

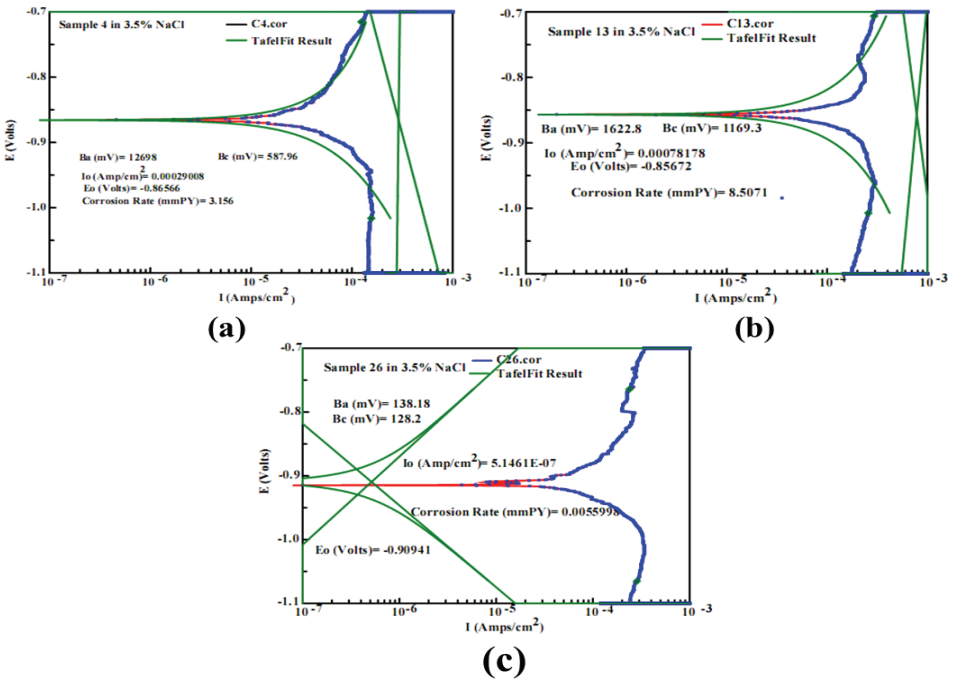

Fig. 5. Tafel plots for the test samples: a) 4 b) 13 and c) 26.

TABLE VI. Corrosion rate of FRSTW samples from potentiodynamic graph

Sample No.	Tafel data				Corrosion rate
	I_{corr} / A cm^{-2}	E_{corr} / V	β_a / mV	β_c / mV	mpy
4	0.00029008	–0.87	12698	587.96	3.156
13	0.00078178	–0.86	1622.8	1169.3	8.5071
26	0.00000052	–0.91	138.18	128.2	0.006

TABLE VII. Weight loss results of some reported aluminum alloys

Aluminum alloy	Welding	Medium	Weight loss g	Duration h	Corr. rate mpy	Ref.
AA6061 and AA8011	FRSTW	Sea water	0.204	672	0.201	2
	FRSTW	HCl	1.644	672	1.618	
	FRSTW	H_2SO_4	1.464	672	1.441	
AA5052-H32 - AA6061-T6	FRSTW	Salt spray	3.77	72	25.486	41

TABLE VII. Continued

Aluminum alloy	Welding	Medium	Weight loss g	Duration h	Corr. rate mpy	Ref.
Al 2024	Raw sample	3.5 % Salt water	–	–	1.200	42
Similar 2219	FRSTW	Salt fog	–	48	0.090	43
Similar 5083	FRSTW	Salt fog	–	48	0.009	43
5083-2219	FRSTW	Salt fog	–	48	0.030	43

CONCLUSIONS

The microstructure, tensile strength, and electrochemical characteristics of friction stir-welded AA5052 and AA6101-T6 were examined in the aforementioned investigations. Three distinct traverse speeds 70, 80 and 90 mm/min, and three distinct rotational speeds 1000, 1200 and 1400 rpm are required for this task. In addition to these three different passes. The nugget zone grain size is exaggerated by process parameters such as tool traverse speed, tool passes and tool traverse speed. Microstructure images have confirmed the solid solution formed between the selected aluminum alloys. The FRSTW tool parameters were modified and successfully this work prepared 29 samples. The sample weight loss results showed that the welding is effectively protecting the metal surfaces in all corrosive medium except salt and alkali medium. In a salt medium, aluminum underwent galvanic corrosion and more weight loss was observed. Likely, in an alkali medium aluminium hydroxide formed, and moderate weight loss was observed. According to potentio-dynamic experiments, AA5052 and AA6101-T6 FRST butt-welds in 3.5 % NaCl solution exhibits improved corrosion control characteristics. The results of the experiments showed that the corrosion current density can be improved by modifying the welding parameters. This work concluded that the 80mm/min–6 kN–1200 RPM–3 passes may be a good parameter for welding and the alloy joint may have higher tensile strength with corrosion resistivity. An evaluation of mechanical properties and electrochemical corrosion performances revealed that the fine and uniform weld microstructure at 1200 rpm outperformed FRSTW joints at 80mm/min in terms of potential, corrosion current density, and tensile strength. The future course study includes the corrosion resistive coating materials according to sacrificial anodic, cathodization and inhibition studies.

Acknowledgment. The authors express their gratefulness to Dr. R. Jayaprakash, Associate Professor, School of Arts and Science, AVIT campus, VMRF, Paiyanoor, Chennai, for his guidance and for providing Vasan R&D lab facility for the corrosion and inhibition studies.

ИЗВОД

ПРОУЧАВАЊЕ КОРОЗИЈЕ, ЕФЕКТИ ПАРАМЕТАРА И ПОВРШИНСКА МОРФОЛОГИЈА AA5052-AA6101T6 ЗАВАРЕНИХ СПОЈЕВА ТРЕЊЕМ И МЕШАЊЕМ

SATHISH RENGARAJAN[1] G. KASIRAJAN[2] и R. ASHOKKUMAR[3]

[1]Department of Mechanical Engineering, St. Joseph's College of Engineering, Semmancheri, Chennai, Tamil Nadu-600119, India, [2]Research Scholar, Department of Mechanical Engineering, St. Joseph's College of Engineering, Semmancheri, Chennai, Tamil Nadu-600119, India и [3]Department of Mechanical Engineering, SRM Madurai College for Engineering and Technology, Nedungulam Main Rd, Pottapalayam, Tamil Nadu-630611, India

Традиционално заваривање фузијом није погодно за заваривање легура алуминијума јер се формирају секундарне крте фазе, а како легура очвршћава јавља се порозност и пукотине. Заваривање трењем, је нова метода заваривања у чврстом стању, којом се могу спојити сличне или различите легуре алуминијума. У овом раду узорци легура AA5052-AA6101T6 који су заварени трењем и мешањем, тестирани су на карактеристике корозије. Микроструктура и механичко понашање заварених спојева алуминијумске легуре AA5052-AA6101T6 испитани су у односу на улазне параметре. Микроструктура открива да брзина заваривања и брзина ротације утичу на микроструктуру шава анализираних узорака заварених површина. Двадесет девет узорака је тестирано на корозију у 3,5 % NaCl, води за домаћинство (880 ppm – SPM), 1 M H_2SO_4, 1 M NaOH и природној морској води током 72 сата. Домаћа слана вода и кисели медијум показали су бољу отпорност на корозију од алкалних и сланих медија. Проучавање отпора показало је благе промене анодног и катодног потенцијала након заваривања трењем.

(Примљено 17. априла, ревидирано 19. маја, прихваћено 24. августа 2024)

REFERENCES

1. Y. Chen, H. Wang, H. Li, X. Wang, H. Ding, J. Zhao, F. Zhang, *Metals* **9** (2019) 718 (https://doi.org/10.3390/met9070718)
2. R. Alfattani, M. Yunus, A. F. Mohamed, T. Alamro, M. K. Hassan, *Materials* **15** (2022) 260 (https://doi.org/10.3390/ma15010260)
3. R. S. Mishra, Z. Y. Ma, *Mater. Sci. Eng. Rep.* **50** (2005) 1 (https://doi.org/10.1016/j.mser.2005.07.001)
4. R. Sathish, A. Sathish Kumar, R. Ashok Kumar, *Bull. Chem. Soc. Ethiop.* **38** (2024) 811 https://dx.doi.org/10.4314/bcse.v38i3.20)
5. J. K. Paik, *Int. J. Nav. Archit. Ocean. Eng.* **1** (2009) 39 (https://doi.org/10.2478/IJNAOE-2013-0005)
6. E. T. Akinlabi, A. Andrews, S. A. Akinlabi, *Trans. Nonferrous Met. Soc. China* **24** (2014) 1323 (https://doi.org/10.1016/S1003-6326(14)63195-2)
7. P. V. Kumar, G. M. Reddy, K. S. Rao, *Def. Technol.* **11** (2015) 362 (https://doi.org/10.1016/j.dt.2015.04.003)
8. V. N. Nguyen, Q. M. Nguyen, H. T. D. Thi, S. C. Huang, *Sādhanā* **43** (2018) 160 (https://doi.org/10.1007/s12046-018-0930-y)
9. R. Pruthviraj, M. Rashmi, *J. Mater. Sci. Eng.* **5** (2016) 1000221 (https://doi.org/10.4172/2169-0022.1000221)
10. B. Ratna Sunil, G. Pradeep Kumar Reddy, Duc Pham, *Cogent Eng.* **3** (2016) 1145565 (https://doi.org/10.1080/23311916.2016.1145565)
11. R. P. Mahto, S. Anishetty, A. Sarkar, O. Mypati, S. K. Pal, J. D. Majumdar, *Met. Mater. Int.* **25** (2019) 752 (https://doi.org/10.1007/s12540-018-00222-x)

12. F. Gharavi, K. A. Matori, R. Yunus, N. K. Othman, F. Fadaeifard, *J. Mater. Res. Tech*. **4** (2015) 314 (https://doi.org/10.1016/j.jmrt.2015.01.007)
13. K. Amini, F. Gharavi, *J. Cent. South Univ.* **23** (2016) 1301 (https://doi.org/10.1007/s11771-016-3180-3)
14. A. Davoodi, Z. Esfahani, M. Sarvghad, *Corros. Sci.* **107** (2016) 133 (https://doi.org/10.1016/j.corsci.2016.02.027)
15. Y. Feng, F. Yang, Y. Bi, *Int. J. Electrochem. Sci.* **17** (2022) 221039 (https://doi.org/10.20964/2022.10.40)
16. S. Khorsand, Y. Huang, in: *Light Metals 2017. The Minerals, Metals & Materials Series*, A. Ratvik, Ed., Springer, Cham, 2017 (https://doi.org/10.1007/978-3-319-51541-0_32)
17. M. Krol, P. Snopinski, B. Tomiczek, T. Tanski, W. Pakiela, W. Sitek, *P. Est. Acad. Sci.* **65** (2016) 107 (https://doi.org/10.3176/proc.2016.2.07)
18. D. A. Wadeson, X. Zhou, G. E. Thompson, P. Skeldon, L. D. Oosterkamp, G. Scamans, *Corros. Sci.* **48** (2006) 887 (https://doi.org/10.1016/j.corsci.2005.02.020)
19. H. Longgang, J. Jiajia, Z. Di, Z. Linzhong, Z. Li, J. Jishan, *Rare. Metal. Mat. Eng.* **46** (2017) 2437 (https://doi.org/10.1016/S1875-5372(17)30212-6)
20. C. Elanchezhian, B. V. Ramnath, P. Venkatesan, S. Sathish, T. Vignesh, R. V. Siddharth, K. Gopinath, *Procedia Eng.* **97** (2014) 775 (https://doi.org/10.1016/j.proeng.2014.12.308)
21. O.M. Khalil, I. Mingareev, T. Bonhoff, A. F. El-Sherif, M. C. Richardson, M. A. Harith, *Opt. Eng.* **53** (2014) 014106 (https://doi.org/10.1117/1.OE.53.1.014106)
22. J. Martin, A. Nominé, V. Ntomprougkidis, S. Migot, S. Bruyère, F. Soldera, G. Henrion, *Mater. Des.* **180** (2019) 107977 (https://doi.org/10.1016/j.matdes.2019.107977)
23. R. H. U. Khan, A. Yerokhin, X. Li, H. Dong, A. Matthews, *Surf. Coat. Tech.* **205** (2010) 1679 (https://doi.org/10.1016/j.surfcoat.2010.04.052)
24. G. Gautam, N. Kumar, A. Mohan, R.K. Gautam, S. Mohan, *J. Mater. Sci.* **51** (2016) 8055 (https://doi.org/10.1007/s10853-016-0076-4)
25. M. Jin, B. Lee, J. Yoo, Y. Jo, S. Lee, *Met. Mater. Int.* (2024) (https://doi.org/10.1007/s12540-023-01594-5)
26. C. Rathinasuriyan, V. S. Kumar, *J. Mech. Sci. Technol.* **31** (2017) 3925 (https://doi.org/10.1007/s12206-017-0738-4)
27. Z. F. Syed, T. R. Tamilarasan, M. S. Dennison, *Aus. J. Mech. Eng.* **21** (2023) 844 (https://doi.org/10.1080/14484846.2021.1914891)
28. K. Chandra, V. Kain, *Eng. Fail. Anal.* **34** (2013) 387 (https://doi.org/10.1016/j.engfailanal.2013.09.007)
29. F. Gharavi, K. A. Matori, R. Yunus, N. K. Othman, F. Fadaeifard, *Trans. Nonferrous Met. Soc. China* **26** (2016) 684 (https://doi.org/10.1016/S1003-6326(16)64159-6)
30. D. E. Newbury, N. W. Ritchie, *Microsc. Microanal.* **21** (2015) 1327 (https://doi.org/10.1017/S1431927615014993)
31. A. Laska, M. Szkodo, D. Koszelow, P. Cavaliere, *Metals* **12** (2022) 192 (https://doi.org/10.3390/met12020192)
32. L. Veleva, *Corrosion Tests and Standards: Application and Interpretation*, R. Baboian, Ed., ASTM International, West Conshohocken, PN (ISBN: 0-8031-2058-3 (2005), pp. 387-404)
33. H. L. Qin, H. Zhang, D. T. Sun, Q. Y. Zhuang, *Int. J. Miner. Metall. Mater.* **22** (2015) 627 (https://doi.org/10.1007/s12613-015-1116-9)
34. F. T. Owoeye, O. R. Adetunji, A. Omotosho, A. P. Azodo, P. O. Aiyedun, *Eng. Rep.* **2** (2020) 12103 (https://doi.org/10.1002/eng2.12103)

35. N. R. Ramesh, V. S. Kumar, *Appl. Ocean Res.* **98** (2020) 102121 (https://doi.org/10.1016/j.apor.2020.102121)
36. E. Aldanondo, J. Vivas, P. Alvarez, I. Hurtado, *Metals* **10** (2020) 872 (https://doi.org/10.3390/met10070872)
37. H. F. Wang, J. L. Wang, W. W. Song, D. W. Zuo, D. L. Shao, *Int. J. Electrochem. Sci.* **11** (2016) 6933 ((https://doi.org/10.20964/2016.08.09)
38. B. I. Attah, R. O. Medupin, T .D. Ipilakyaa, U. G. Okoro, O. Adedipe, G. Sule, O. M. Ikumapayi, K. C. Bala, E. T. Akinlabi, S. A. Lawal, A. S. Abdulrahman, *Manuf. Rev*. **11** (2024) 7 (https://doi.org/10.1051/mfreview/2024003)
39. Y. Wang, H. Jiang, X. Wu, Q. Meng, *Crystals* **13** (2023) 582 (https://doi.org/10.3390/cryst13040582)
40. R. Saravanakumar, T. Rajasekaran, C. Pandey, *J. Mater. Eng. Perform.* **32** (2023) 10175 (https://doi.org/10.1007/s11665-023-07836-2)
41. S. Balamurugan, K. Jayakumar, A. S. Banu, K. Ragupathi, *Eng. Proc.* **61** (2024) 12 (https://doi.org/10.3390/engproc2024061012)
42. M. Starostin, G. E. Shter, G. S. Grader, *Mater. Corros.* **67** (2016) 387 (https://doi.org/10.1002/maco.201508552)
43. M. Koilraj, A. Sathesh Kumar, D. L. Belgin Paul, S. R. Koteswara Rao, *Appl. Mech. Mater* **813**–**814** (2015) 203 (https://doi.org/10.4028/www.scientific.net/AMM.813-814.203).